Lateral Force on Fingertips by Traveling Waves in a Flat Structure Based on the Ultraloop

Master Thesis

Koen Johannes Renkema

TU Delft

Lateral Force on Fingertips by Traveling Waves in a Flat Structure Based on the Ultraloop

by

Koen Johannes Renkema

to obtain the degree of Master of Science
at the Delft University of Technology,
to be defended publicly on Thursday 1st of June, 2023 at 9:30 AM.

Student number:	4603451	
Project duration:	September, 2022 – June, 2023	
Thesis committee:	Dr. M. Wiertlewski,	TU Delft, supervisor, chair
	Z. Cai, MSc,	TU Delft, supervisor
	Prof.dr P. Steeneken,	TU Delft, external committee member

An electronic version of this thesis is available at `http://repository.tudelft.nl/`.

TU Delft

Lateral Force on Fingertips by Traveling Waves in a Flat Structure Based on the Ultraloop

Koen Renkema

***Abstract*—Creating a lateral force on a finger touching a touchscreen can provide the sensation of a bump in the surface, and generate a pulling sensation, which could enhance the experience of operating a touchscreen. The Ultraloop, a device built to generate such a lateral force on a finger in contact, works by producing flexural traveling waves that push the finger. However, its shape is not simple to manufacture. Moreover, its shape is inconvenient to place in most touch input interfaces, which often appear in flat devices. A flat UltraLoop is proposed providing similar traveling wave force feedback, fitting the form factor of flat human-machine touch interfaces better. Furthermore, the new shape allows for manufacturing from a sheet of aluminum, using a cnc. The flat Ultraloop works by actuating two orthogonal modes at around 38k Hz, with a phase shift of 90 degrees, similarly to the Ultraloop. To validate the performance, force measurements have been conducted showing a maximum lateral force of 0.3N. Also, the influence of the normal force, phase, and finger motion on the lateral force is investigated. Lastly, we present a demo showing application of the flat Ultraloop, simulating a spring and a bump.**

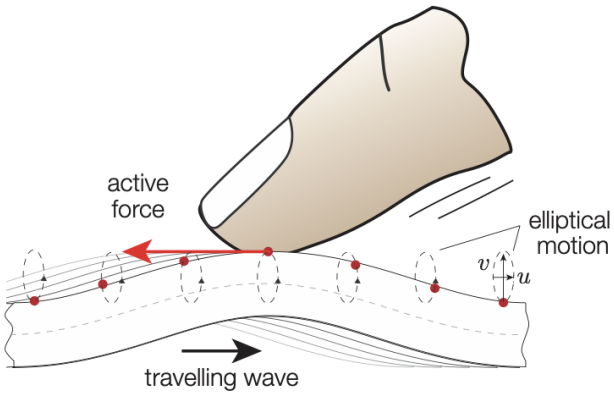

Fig. 1. A surface in a traveling wave exerts a force F on the finger, which direction is opposite to the propagation of the wave. The surface particles follow an ellipsoid path, resulting in the asymmetric force which generates the net lateral force.[9]

I. Introduction

Touch input based interfaces like trackpads, touchscreens and capacitive buttons are prevalent nowadays. They can be found in computers, self checkouts in grocery stores, and home appliances, providing a natural way of interacting with modern devices. Since touch input interfaces are plain flat surfaces, a displayed button cannot be found blindly, nor interaction with that button can be felt. Visual attention is always needed to operate a touch input interface. Older input devices such as physical buttons, knobs and sliders have two advantages over touch input ingrained in their design: the tactile feedback when a button is pressed or knob turned, and their 3d shape, enabling the user to find them blindly.

Touch input interfaces are therefore often equipped with vibrotactile or auditory feedback, to alert the user when input such as a button click is received. However, this does not help finding a displayed button on a screen blindly, which comes apparent when using a touch input device while vision is limited or impossible. For example, while driving a car equipped with a touchscreen, it is desirable to find a displayed temperature slider or volume knob blindly on the screen, to prevent getting distracted from the road. Moreover, visually impaired individuals experience significant challenges operating a touch input interface [1], which is a problem in a society where many human-machine interfaces are touch-input based. It would therefore be beneficial to add tangible feedback on the flat surfaces of touch input devices, aiding interaction with the displayed interface.

Currently, methods exist to create such sensation of shapes and buttons on a flat surface, called surface haptics. Surface haptics makes use of the illusion that sliding a finger over a surface which modulates the lateral (in-plane with the surface) force will be perceived as if the surface has a bump, hole or texture, dependent on how the force changes over distance [2] [3]. The first type of surface haptics modulates the force between the finger and surface by changing the friction. The friction can be changed in two ways: using ultrasonic vibration, or electroadhesion. An ultrasonic out-of-plane vibration creates a squeeze film of air [4, 5, 6, 7], resulting in air lubrication decreasing the friction. Alternatively, electroadhesion is achieved by inducing a voltage potential between the fingertip and surface [8], which increases the friction. Because these techniques rely on friction modulation, movement of the finger is required in order for the effect to be noticeable, which is why this type of surface haptics is called passive surface haptics. For passive surface haptics to work, movement of the finger is necessary, since it relies on changing the friction between the finger and surface. Also, the resulting modulated friction force can only act in the counter direction of the movement of the finger. While this is sufficient for simulating textures or bumps, it does not work on a static finger. If we want to push a finger in a certain direction for guidance, or create the sensation that the finger rests against a button, the surface needs to actively exert a net lateral force on the fingertip.

The generation of a net lateral force on a finger, independent of the movement of the finger, is called active surface haptics. Such a force can be created by using asymmetric friction, by synchronizing friction modulation with in-plane vibrations of

the surface causing an asymmetric force profile, or net lateral force. For the friction modulation, either ultrasonic vibrations [10] or electroadhesion [11] can be used. However, the in-plane vibration frequency of previously mentioned devices is audible. To avoid this audible noise, UltraShiver [12] vibrates at an ultrasonic frequency. A maximum lateral force of 450 mN was reached, however, the high frequency vibration results in a non-uniform vibration profile, causing a non-uniform force profile over the surface. Using different modes of vibration solved this, however resulted in a lower lateral force of 300 mN [13]. Another method for creating a lateral force, is by vibrating a surface in both in-plane and out-of-plane direction at the same frequency like the LateralPaD [14]. The resulting movement of the surface follows a line, and the devices produces a small lateral force of 70 mN. Another strategy to create a lateral force on a finger, is by using the elliptical motion of a beam's surface in a traveling flexural wave. [15, 16] (figure 1). This principle is used in ultrasonic motors, but also touching the vibrating part of the motor was found to generate lateral force on the finger [17]. A surface particle at its highest point has a velocity relative to the finger in the direction of the force, while at its lowest point the point moves against the direction of the force. A traveling wave in a straight beam can be generated by using two Langevin transducers [15], resulting in a lateral force of ±0.1N. A more efficient strategy is by using the resonance of a ring-type structure such as the UltraLoop [9], creating a lateral force of ±0.3N.

The Ultraloop's shape consists of two semicircles with a radius of 50 mm, connected by two straight beams of 140 mm. The width is 30 mm, while the thickness is 2.75mm. However, the Ultraloop's design holds two problems. Firstly, the 3D shape will not be practical to apply in flat devices such as trackpads and tablets, since the Ultraloop's total height is 102.75 mm. Secondly, electrical discharge machining is needed to manufacture the UltraLoop, which is expensive and time consuming. In this paper, a flat version of the UltraLoop is reported. The rectangular touchable surface measures 30×80 mm , or 80×140 mm when including the two ends with nonuniform thickness connecting to the banked corner. The device is capable of exerting a lateral force (0.3N) on a finger in contact, similar to the Ultraloop. The flat Ultraloop is compared to its original by comparing the modeshapes measured by a laser-Doppler vibrometer (LDV), and force measurements. The flat version of the Ultraloop is easier to manufacture, and uses less 3D space than the Ultraloop. To demonstrate the effectiveness of the device, a demo is built. By recording the finger position and altering the lateral force acting on the finger accordingly, different effects and shapes can be realized to clearly substantiate the force acting on the finger.

II. Design of a flat traveling wave structure

A. Traveling Waves

To understand the generation of a traveling wave, first a traveling wave in a line is explained. The transverse displacement of a bending wave traveling along the x axis can be described as

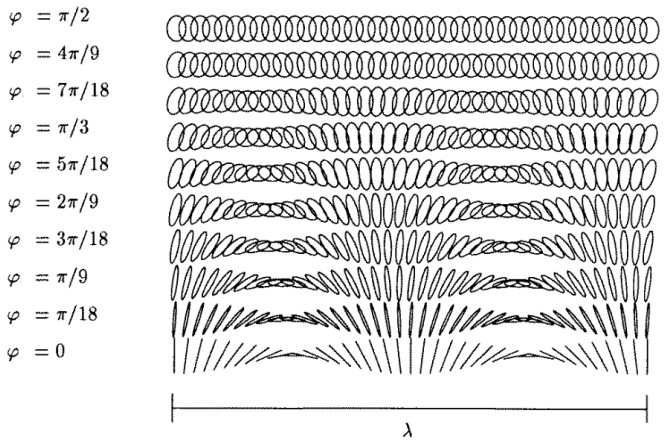

Fig. 2. Movement of surface particle for different phase shifts φ [16]. For $\varphi = 2/\pi$, the beam is in a purely traveling wave, and the surface particles follow the same ellipsoid trajectory. For a phase shift of $\varphi = 0$, the wave in the beam is purely standing, and the trajectory followed by the surface particles is a line, which direction depends on the location in the wave: at a node, the movement is purely longitudinal, whereas at an antinode, the movement is purely in the normal direction.

$$v(x,t) = C\ cos(kx - \omega t) \tag{1}$$

where ω is the frequency and C is the amplitude. A traveling wave can be realized by the superposition of two standing waves, since from the trigonometric identities we know:

$$sin(A)sin(B) + cos(A)cos(B) = cos(A - B) \tag{2}$$

where we can recognize two summed standing waves described in the left hand side of the equation, by letting A and B represent the spatial and temporal dimension of the waves respectively, resulting in the following formula:

$$sin(kx)sin(\omega t) + cos(kx)cos(\omega t) = cos(kx - \omega t). \tag{3}$$

Hence, a purely traveling wave can be realized by superposition of two standing waves of the same frequency, with a phase difference of 90° or $\frac{1}{2}\pi$ in both time and space, since $\angle sin(\alpha) - \angle cos(\alpha) = \frac{1}{2}\pi$.

A simple traveling wave in a line is described by equation 13, however when adding a thickness to this line, the movement becomes more complicated. According to the Euler–Bernoulli beam theory, a cross-section of the beam is always perpendicular to the axis of the beam, allowing us to express the exact transverse and longitudinal displacement of any point in the traveling wave [16]. Since the cross-section is perpendicular to the center line, we know that the lateral displacement $u(x,z,t)$ is the slope of the center line $v(x,t)$ multiplied by the distance z from the center line:

$$u(x,z,t) = -zv'(x,t) = -Czk\ sin(kx - \omega t) \tag{4}$$

Squaring and summing $u(x,z,t)$ and $w(x,t)$ gives the relation between the axial and transverse displacement:

$$\frac{u^2}{(Czk)^2} + \frac{v^2}{C^2} = cos^2(kx - \omega t) + sin^2(kx - \omega t) = 1. \tag{5}$$

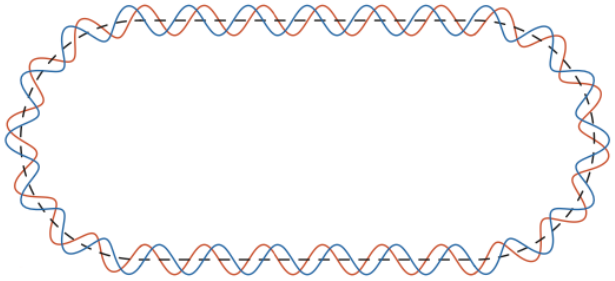

Fig. 3. 24th Mode along the center line of the Ultraloop

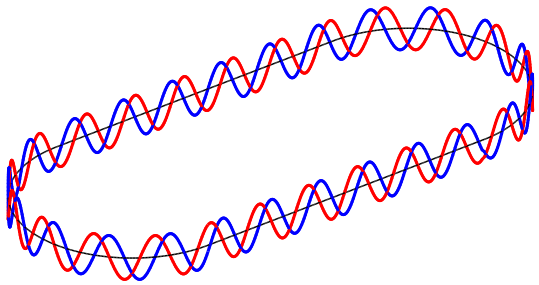

Fig. 4. The modeshape along the center line of the flat Ultraloop.

Since Eq. (6) describes an ellipse, it is clear that a surface particle at $(x, z = h/2)$ will follow an ellipsoid path.

If phase difference φ in time in eq.3 and eq.4 is not 90 degrees, the resulting wave won't be purely traveling. At $\varphi = 0$ and 180 degrees, the resulting wave will be standing, and the surface particles move along a line instead of an ellipse. This is illustrated for different values of φ in figure 2.

B. Current ring-type traveling wave structure

A continuous traveling wave cannot exist in a simple finite plate, because the reflection of waves at the edges will distort the traveling wave, eventually resulting in a standing wave. To prevent this distortion, a looped ring-type structure can be used to generate a traveling wave [18] such as the Ultraloop [9]. The Ultraloop consists of two straight slabs connected by two semicircular beams, all with the same thickness and width. The dimensions of the Ultraloop have been designed using Euler-Bernoulli beam theory and Hamilton's principle. Using a sinusoidal mode shape (24th mode) along the center line (figure 3), the dimensions providing two close resonance frequencies giving two orthogonal modes are found. Since the distance between the two modes is $\frac{1}{4}\lambda$, according to eq. 4 it is possible to generate a traveling wave, by simultaneously driving the two modes with a temporal phase difference of $\varphi = 90$. Placing piezoelectric actuators on the antinodes of the two modes allows driving both modes separately. The two modes have a slightly different resonance frequency, and since the amplitude of both modes should be equal, the driving frequency is the average of both resonance frequencies. The same technique will be used for the flat Ultraloop: finding the same 24th mode in a flat ring-type shape, with two orthogonal modes with close by resonance frequencies.

C. Flat Ultraloop design

As a basis, the same dimensions of the original UltraLoop have been used, the center line is exactly the same. This similarity means that the 24th mode shape which was used for the Ultraloop can also be applied to the flat counterpart. However, for the flat Ultraloop the transverse motion of the wave is in the direction out of the plane of the center line, see figure 4. The second difference is that, for the Ultraloop, the

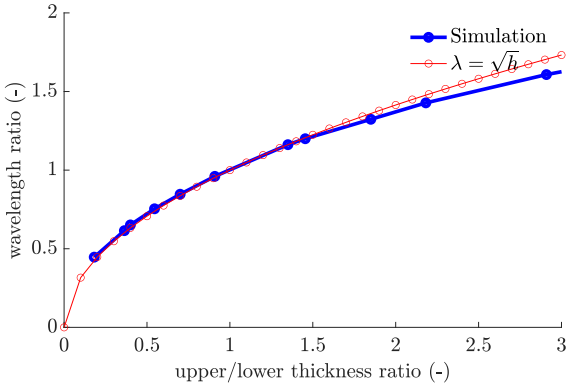

Fig. 5. For each change in thickness, the change in wavelength can be observed to follow the function $\lambda = \sqrt{h}$. For higher ratios there is some deviation, however at the range of interest (wavelength ratio = 0.7-1.3) the deviation is negligible.

distance around the structure is the same at different values of y. The flat Ultraloop however introduces different path lengths along the width of the structure in the bends, and thus the phase velocity should be manipulated to be dependent on the local radius, effectively resulting in an equal number of waves on the inside as the outside bend.

We can modulate the wavelength in the corners by simplifying the formula describing the wave number k [19]:

$$k = \frac{2\pi}{\lambda} = \omega^{\frac{1}{2}} \left(\frac{\rho A}{EI}\right)^{\frac{1}{4}} \tag{6}$$

where λ is the wavelength, ρ and E are the density and Young's modulus of the medium respectively, and I is the moment of inertia of the cross-sectional area A.Assuming constant frequency ω, and given $A = w * h$, simplifying equation 6 gives the relation between wavelength λ and thickness h:

$$\lambda \propto \sqrt{h} \tag{7}$$

In Comsol, by running simulations for different changes in thickness of a Ultraloop, this relation was validated. For example, when the thickness changed with a factor two, the change in wavelength was $\sqrt{2}$ (see figure 5). Since we can manipulate the wavelength by changing thickness h, a

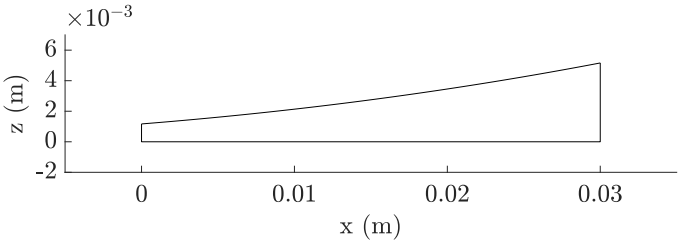

Fig. 6. The cross-section of the corner, described by equation 9.

quadratic thickness profile will result in equal amount of waves in the inner and outer bend. The thickness profile is described by:

$$h(r) = h_{straight}(\frac{r}{R})^2 \tag{8}$$

where $h_{straight}$ is the thickness of the structure in the straight part and along the center line, r is the local radius and R is the radius of the corner of the center line. Several Comsol simulations have been conducted in order to find the dimensions resulting in a high displacement traveling wave. Another important criterion was the shape of the waves: the flexural waves in the straight part (also touch area) of the device should be mostly in y direction, creating straight node lines in the y direction for both orthogonal standing waves (figure 7). To guide the wave such that the node lines are straight, the inner and outer side of the wave should arrive at the same time at the straight part. The first simulation showed more nodes along the outside bend than the inside bend, suggesting that the change in thickness along the width in the corner was insufficient. The thickness profile

$$h(r) = 0.00275(\frac{r}{0.05})^{2*1.2} \tag{9}$$

was found to result in the best looking modeshape, and can be observed in figure 6. The added power of 1.2 results in even larger wavelengths for the outside bend, and smaller wavelengths in the inside bend, which was found to be necessary for the waves maintaining perpendicular to the center line in Comsol.

To connect the 'banked' corners to the straight part of the flat Ultraloop, the thickness gradually changes at the transition parts, measuring 0.03×0.03 m. The device is assembled from an aluminum plate, using a cnc machine.

D. Validation

To validate whether the modeshape of the flat Ultraloop matches the modeled modeshape in Comsol, the device's vibration amplitude is measured with a laser Doppler vibrometer (LDV).

1) Bode Plot: Using the LDV, the surface velocity was measured for each channel during a frequency sweep. The signal was created in Matlab, and generated by a daq (NI USB-6351) sending the signal to the two amps (PiezoDrive PD200) for both channels, see figure 8.

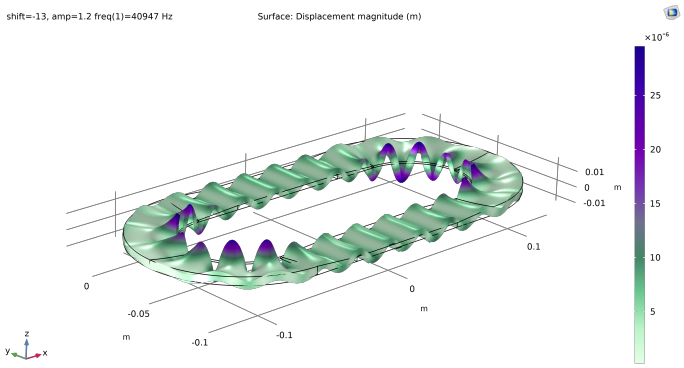

Fig. 7. The resulting modeshape simulated in Comsol

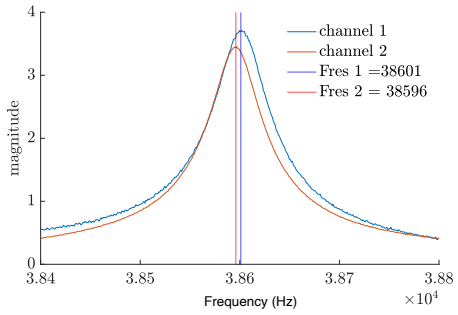

Fig. 8. The bode plots of channel 1 and 2 show close by resonance frequencies.

2) Surface Plot: At the resonance frequencies, it is desired to inspect the modeshape of the device. Measuring the surface velocity at a grid of points on the devices' touch surface allows the creation of surface plots showing the modeshape (figure 9). Since we expect the waves to be mostly visible along the y axis, this stepsize of the grid is smaller in the y direction ($0.001m$) than x direction ($0.005m$). Again, the signal at the resonance frequency is generated by a the daq and amplified. The LDV measures the surface velocity, and a galvo is used to track all points on the grid. Contrary to expectation, the nodelines of the standing waves are not straight. Also, a lot of fluctuation in amplitude is visible for the traveling wave.

III. Results

Four different force measurements have been conducted, to understand the effect of location x, normal force F_N, phase ϕ and movement on the lateral force F_x. Furthermore, a demonstration setup has been built that works by making the force F_x on the finger dependent on the finger position, allowing to generate tangible effects and features on the surface.

A. Force Measurement Setup

The flat UltraLoop is mounted onto a plate, which rests solely on a 6 axis force sensor (HEX32 by Wittenstein), which is then mounted to a ground plate. The Ultraloop is mounted

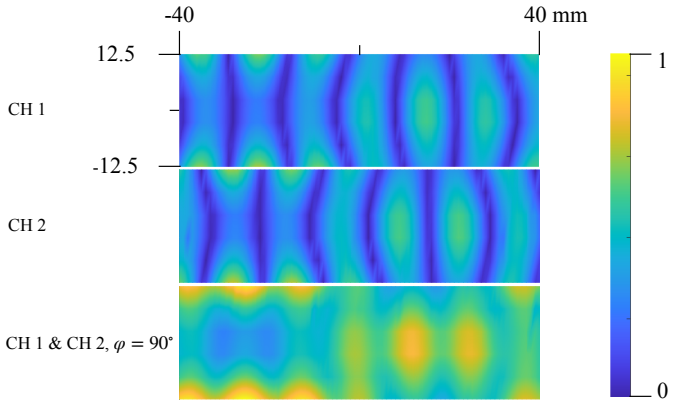

Fig. 9. Modeshape of the two ortogonal standing waves and the traveling wave, where both channels are actuated with a phase shift of 90°. The traveling wave shows no lines with zero displacement, however it does not display a pure traveling wave.

such that the straight touchable surface is centered above the force sensor. From the ground plate, a perpendicular plate is mounted, holding a extrusion profile which holds a finger holder preventing the human to exert additional/external lateral force during measurements. For example, if a force in the direction to the left is measured on the finger, the finger will be placed on the right side of the finger holder. For driving the piezoelectric actuators, a Tektronix AFG1062 function generator is used to generate two signals, for the two arrays of actuators. The output of the function generator is $6V_{pp}$, which is not enough for our application. For amplification, an amplifier (PiezoDrive PD200) is used per channel to amplify the signal to $V_{pp} = 120$. Changes in temperature causes expansion of the material, which also changes the resonance frequency. The resonance frequency is determined using the LDV prior to each measurement, after which both channel 1 and channel 2 are driven at that frequency. For all force measurements excluding the sliding measurement, the lateral force has to be modulated in order to measure the change in lateral force between 'off' and 'on'., the force was turned on and off by modulating the phase. Modulating the amplitude to turn off the force would result in the surface becoming more sticky, and the finger skin not being able to move back to its rest position. Since the finger would thereby be pulled against the finger holder, the change in lateral force could not be measured. By modulating the phase to 0, the surface is essentially acting as a friction modulation device. This low friction surface allows the skin to move back, removing the built up lateral force.

B. Lateral force at center line

The lateral force is measured along the center line of the straight part, to evaluate how much the force changes along this line. The force was measured at $x = -0.04 : 0.01 : 0.04$. For each trial, the finger was placed on the left side of the finger holder, in order to prevent the finger moving to the right due to the induced lateral force. A constant normal force of approximately $1N$ was held by the researcher. By alternating between a 0 and 90 degrees phase shift, the force induced by the traveling wave can be measured by subtracting the lateral forces: $F_x = F_{x,measured}(\varphi = 90) - F_{x,measured}(\varphi = 0)$. During each trial, the phase changes from 0 to 90 6 times. With 3 trials per location, this results in 18 force measurements per location, which can be seen in figure 10. The results show

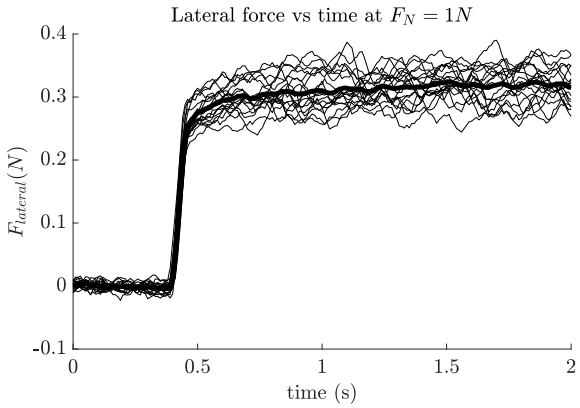

Fig. 10. All force measurements at location $x = 0.03$ at $F_N = 1N$

large discrepancies in lateral force at different locations on the center line. At $x = -0.03$ and $x = -0.02$

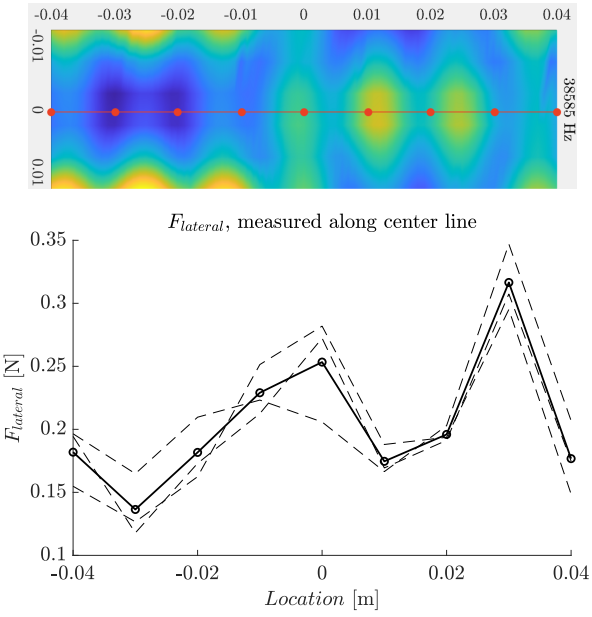

Fig. 11. Lateral force at different locations x. Dotted lines are averages per trial, the continuous line displays the total average force.

C. Lateral vs normal force

To investigate the influence of normal force on the lateral force, the lateral force F_x has been measured for different normal forces F_N, at $x = 0.03$ (figure 12 . A trial consisted

of first applying a normal force of $F_N = 0.2, 0.5, 0.8, 1, 1.5$ and $2N$. Secondly, the phase was alternating between 0 and 90 degrees 8 times, so the change in lateral force could be measured. For each normal force, 3 trials were conducted.

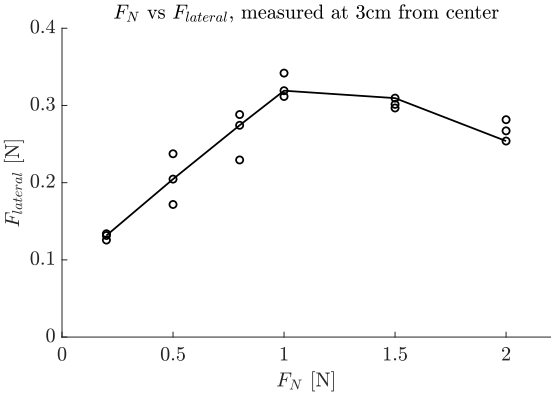

Fig. 12. Lateral force vs normal force, measured at 3 cm from center.

For all measured $F_N \leq 1N$ the lateral force F_x scales linearly with F_N. For $F_N > 1N$, the lateral force F_x decreases slightly for higher values of F_N. At $F_N = 1N$ the average lateral force is $F_x = 0.31N$

D. Lateral force vs phase

Similarly, F_x has been measured by looping over the phase difference φ with increments of 10. For $\varphi = [0, 180]$, resulting in a negative lateral force, the finger was placed to the left of the finger holder to prevent external lateral force. For $\varphi = [190, 360]$, the finger was placed on the right side of the finger holder. The lateral force changes with respect to φ, reaching

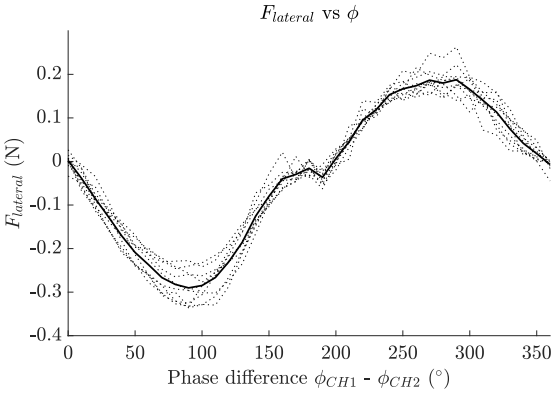

Fig. 13. Lateral force $F_{lateral}$ for different values of phase ϕ. Since $F_{lateral}$ changes when altering ϕ, it is possible to change the magnitude and direction of $F_{lateral}$ solely by modulating ϕ.

0N at 0, 180 and 360 degrees, and reaching maxima at $\varphi = 90$ and 270 degrees, resulting in approximately $0.3N$ and $0.2N$ of force respectively.

E. Lateral force during sliding

To evaluate the lateral force on the finger during gestures, the lateral force can be measured while sliding in both directions. During measurements, the researcher tried to maintain

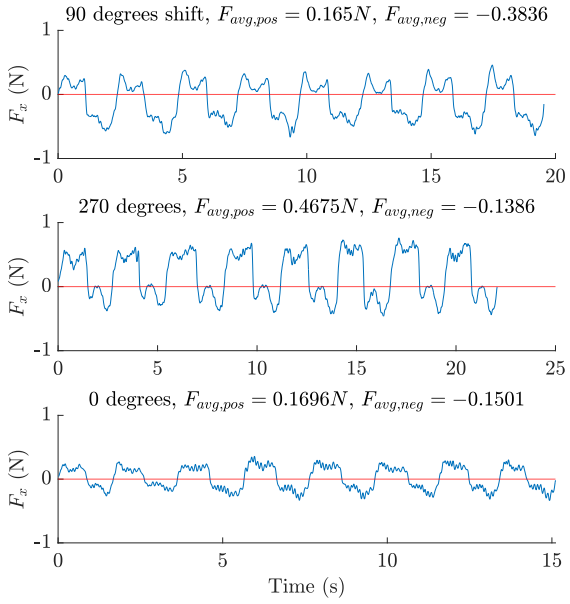

Fig. 14. Typical trials for swiping to the left and right, for $\varphi = 90, 270$ and 0. A lateral force of $0N$ is indicated in red.

a constant normal force, similar to as if they were swiping a regular touch screen surface. Since the lateral force is 0 when switching directions, it is possible to distinguish a left from a right stroke (figure 14). At $\varphi = 90$, the lateral force while swiping to the right averages at $F_x = 0.165N$. While swiping to the left, the force is $F_x = -0.3836N$. Here, a right swipe is in the direction of the force, and a left swipe moves against the force. At $\varphi = 270$, the direction of the force is switched. Swiping to the right results in $F_x = 0.4675N$, swiping to the left generates $F_x = -0.1386N$. As a baseline, the lateral force was measured at $\varphi = 0$, creating a lateral force of $F_x = 0.1696N$ and $F_x = -0.1501N$ for a right and left stroke respectively.

F. Demo

By adding a infrared position sensor (Neonode NNAMC1580PCEV), we can create force feedback dependent on the finger position by modulating the phase φ . A bump and a spring have been simulated, to demonstrate the tangibility of the force. The setup with the position sensor can be seen in figure 15

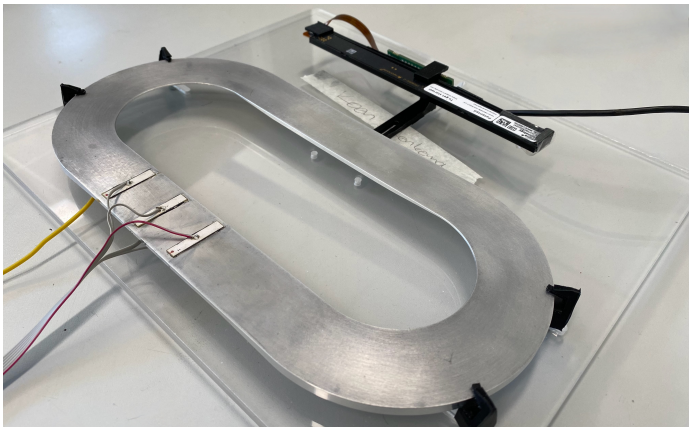

Fig. 15. Demo setup with position sensor

IV. Discussion

In this study, changing the shape of the Ultraloop from the original ring shape a flat one has been investigated. The new design has been tested in 2 different ways: by measuring the modeshape using a LDV, and by force measurements.

A. Design

The modeshape that was measured by the LDV (figure 9) shows non-straight node lines, different from modeshapes observed during simulation in comsol. A possible explanation to this modeshape is that closeby resonance frequencies are actuated simultaneously, causing vibration in not only the x but also y direction along the straight part. Another interpretation is that the design of the corner causes the waves in the inside and outside bend not to arrive simultaneously, resulting in the waves not being straight in the straight part. Since this mode shape was not observed in the Comsol simulations, it is possible that the corner is not designed or manufactured properly. Different thicknesses or cross-section profiles should be tested to find the correct shape for modeshapes with purely bending waves around the y axis in the straight part.

One problem with using aluminum as material to carry the vibration, is that temperature differences cause big fluctuations (±100 Hz) in the resonance frequencies of the two modes. Using the device for more than a minute will cause it to heat up, resulting in worse performance. One solution has been found in Ultrasonic Motors, by monitoring the phase difference between the two modes. This could also be implemented for the Ultraloop and flat Ultraloop, to ensure a constant optimal working frequency.

B. Force measurements

Several irregularities can be observed in the force measurements: the force fluctuates along the center line, the maximum negative lateral force is higher than the maximum positive lateral force, and a swipe to the right results in a larger lateral force than a swipe to the left, when moving in the counter direction of the generated lateral force. A possible explanation is that the conditions of the finger and surface were not equal for all measurements. After wiping the surface with alcohol, the effect was sometimes perceived more clearly. This suggests that the conditions such as cleanness of the surface, and probably the finger, have an influence on the force. This is not strange, since generating the force relies on the friction between the finger and surface. For more consistent measurements, a fake finger could be used. Dependence on surface and skin conditions introduces a problem that sometimes the effect is not as perceivable, making the technology less usable. Another possible variable is the contact surface. While the researcher tried to position the finger similarly every time, some variation is still possible, since contact area is dependent on the angle of the finger.

1) Lateral force at center line: The measured maximum lateral force that the flat Ultraloop is able to produce, is similar to the maximum force of the Ultraloop. However, this highest force does not occur everywhere along the center line, where the force was measured. The measured vibration amplitude also shows quite some fluctuation, while for a pure traveling wave the amplitude should be uniform. Along the center line, we observe that for a lower vibration amplitude, the measured force is also lower. However, this does not explain the peak at x=0.03, since no big peak in vibration amplitude is present there. In the future, the shape of the flat UltraLoop should be optimized, to generate modeshapes with pure flexural waves, resulting in a more uniform lateral force on the surface.

2) Lateral force vs normal force: The normal force has an interesting influence on the lateral force. The peak of the lateral force at $F_N = 1N$ can be explained. First, the lateral force increases linearly with the normal force, since the lateral force is dependent on the friction between the finger and surface. This friction force increases linearly. However, for $F_N > 1N$, the absorption of energy of the flat Ultraloop into the finger can result in a lower vibration amplitude, and thus a lower lateral force.

3) Lateral force vs phase: The phase between the two channels has a direct effect on the traveling wave ratio, and thus the lateral force. We can use this to modulate the force, without changing the amplitude of the signals.

4) Lateral force during sliding: As expected, when sliding against the direction of the produced lateral force, the force on the fingertip is larger than while sliding in the same direction of the force. This shows that it is possible to provide force feedback during sliding. However, it has not been tested whether the force is also present while sliding orthogonal to the force.

V. Conclusion

In this paper, we present a flat version of the Ultraloop, able to generate a lateral force of $0.3N$ at a normal force $F_N = 1N$ of on the fingertip, which matches the performance of the original. The flatter structure fits more easily in flat touch input devices such as trackpads and tablets.

The object of this research was to investigate the possibility of creating a flat version of the Ultraloop. By using the same center line dimensions, the device could be designed to have

the same 24th mode, by using banked corners to correctly guide the wave. This resulted in a traveling wave providing lateral force, which can be used to provide force feedback to a finger.

By changing the phase φ between the two channels, the resulting force can be modulated. When adding a position sensor, the force on the finger can be dependent on the user's finger motion, allowing force feedback on a surface. This was demonstrated with a demo, where the user can feel a spring and a bump being simulated.

REFERENCES

[1] Shaun K Kane, Meredith Ringel Morris, and Jacob O Wobbrock. Touchplates: low-cost tactile overlays for visually impaired touch screen users. In *Proceedings of the 15th International ACM SIGACCESS Conference on Computers and Accessibility*, pages 1–8, 2013.

[2] Gabriel Robles-De-La-Torre and Vincent Hayward. Force can overcome object geometry in the perception of shape through active touch. *Nature*, 412(6845):445–448, 2001.

[3] Allan M Smith, Georges Basile, Jonathan Theriault-Groom, Pascal Fortier-Poisson, Gianni Campion, and Vincent Hayward. Roughness of simulated surfaces examined with a haptic tool: effects of spatial period, friction, and resistance amplitude. *Experimental brain research*, 202:33–43, 2010.

[4] Nicholas D Marchuk, J Edward Colgate, and Michael A Peshkin. Friction measurements on a large area tpad. In *2010 IEEE Haptics Symposium*, pages 317–320. IEEE, 2010.

[5] Su Zhao, Sebastian Mojrzisch, and Joerg Wallaschek. An ultrasonic levitation journal bearing able to control spindle center position. *Mechanical Systems and Signal Processing*, 36(1):168–181, 2013.

[6] Melisande Biet, Frederic Giraud, and Betty Lemaire-Semail. Squeeze film effect for the design of an ultrasonic tactile plate. *IEEE Transactions on Ultrasonics, Ferroelectrics, and Frequency Control*, 54(12):2678–2688, 2007.

[7] Michaël Wiertlewski, Rebecca Fenton Friesen, and J Edward Colgate. Partial squeeze film levitation modulates fingertip friction. *Proceedings of the national academy of sciences*, 113(33):9210–9215, 2016.

[8] Olivier Bau, Ivan Poupyrev, Ali Israr, and Chris Harrison. Teslatouch: electrovibration for touch surfaces. In *Proceedings of the 23nd annual ACM symposium on User interface software and technology*, pages 283–292, 2010.

[9] Z. Cai. Ultraloop: a traveling wave generator for excerting lateral force on the fingertip.

[10] Erik C Chubb, J Edward Colgate, and Michael A Peshkin. Shiverpad: A glass haptic surface that produces shear force on a bare finger. *IEEE Transactions on Haptics*, 3(3):189–198, 2010.

[11] Joseph Mullenbach, Michael Peshkin, and J Edward Colgate. eshiver: Lateral force feedback on fingertips through oscillatory motion of an electroadhesive surface. *IEEE transactions on haptics*, 10(3):358–370, 2016.

[12] Heng Xu, Michael A Peshkin, and J Edward Colgate. Ultrashiver: Lateral force feedback on a bare fingertip via ultrasonic oscillation and electroadhesion. *IEEE transactions on haptics*, 12(4):497–507, 2019.

[13] Heng Xu, Michael A Peshkin, and J Edward Colgate. Switchpad: Active lateral force feedback over a large area based on switching resonant modes. In *Haptics: Science, Technology, Applications: 12th International Conference, EuroHaptics 2020, Leiden, The Netherlands, September 6–9, 2020, Proceedings 12*, pages 217–225. Springer, 2020.

[14] Xiaowei Dai, J Edward Colgate, and Michael A Peshkin. Lateralpad: A surface-haptic device that produces lateral forces on a bare finger. In *2012 IEEE Haptics Symposium (HAPTICS)*, pages 7–14. IEEE, 2012.

[15] Sofiane Ghenna, Eric Vezzoli, Christophe Giraud-Audine, Frédéric Giraud, Michel Amberg, and Betty Lemaire-Semail. Enhancing variable friction tactile display using an ultrasonic travelling wave. *IEEE transactions on haptics*, 10(2):296–301, 2016.

[16] W Seemann. A linear ultrasonic traveling wave motor of the ring type. *Smart materials and structures*, 5(3):361, 1996.

[17] Mélisande Biet, Frédéric Giraud, François Martinot, and Betty Semail. A piezoelectric tactile display using travelling lamb wave. 2006.

[18] Xinchang Liu, Dan Shi, Yoan Civet, and Yves Perriard. Modelling and optimal design of a ring-type structure for the generation of a traveling wave. In *2013 International Conference on Electrical Machines and Systems (ICEMS)*, pages 1286–1291. IEEE, 2013.

[19] Minoru Kuribayashi, Sadayuki Ueha, and Eiji Mori. Excitation conditions of flexural traveling waves for a reversible ultrasonic linear motor. *The Journal of the Acoustical Society of America*, 77(4):1431–1435, 1985.